Mechanisms of epitaxial growth and magnetic properties of γ'-Fe_4N(100) films on Cu(100)

J. M. Gallego
Instituto de Ciencia de Materiales de Madrid, CSIC, Cantoblanco, 28049, Madrid, Spain

S. Yu. Grachev and D. M. Borsa
NVSF, Materials Science Centre, University of Groningen, Nijenborgh 4, 9737 AG, The Netherlands

D. O. Boerma
Departamento de Física de la Materia Condensada, Universidad Autónoma de Madrid, Cantoblanco, 28049, Madrid, Spain and Centro de Micro Análisis de Materiales, Universidad Autónoma de Madrid, Cantoblanco, 28049, Madrid, Spain

D. Écija and R. Miranda
Departamento de Física de la Materia Condensada, Universidad Autónoma de Madrid, Cantoblanco, 28049, Madrid, Spain
(Received 18 March 2004; published 24 September 2004)

Thin films of iron nitride have been grown on Cu(100) single-crystals by molecular beam epitaxy of Fe in the presence of a beam of atomic N provided by a radio-frequency plasma source. Under the appropriate growth conditions, the films are high-quality, epitaxial, single-phase γ'-Fe_4N (100). The mechanisms of growth have been studied from the early stages by scanning tunneling microscopy, low energy electron diffraction and Auger electron spectroscopy, that show that the interface with the Cu substrate is very sharp, the intermixing between the growing film and the Cu substrate being limited to few monolayers. The film grows layer by layer. Mössbauer spectroscopy and Kerr effect measurements confirm that the films are magnetic at room temperature, with the easy axis in the plane of the film and parallel to the ⟨100⟩ direction.

DOI: 10.1103/PhysRevB.70.115417 PACS number(s): 68.37.Ef, 68.55.−a, 75.50.Bb

I. INTRODUCTION

The nitrides of iron have since long played an important role in steel technology. In particular, nitriding is used to harden iron surfaces and to passivate them against oxidation.[1] In addition, the magnetic properties of the iron nitrides with small N content, in combination with their favorable corrosion and wear properties, have raised considerable interest concerning applications for magnetic data storage.[2,3] As an example, soft magnetic layers of nanocrystalline iron nitrides with low losses in GHz frequency applications can be produced.[4]

The Fe-N system has a rather complex phase diagram which nitrogen-poor side is shown in Fig. 1.[5,6] Since all Fe nitrides are metastable with respect to decay into N_2 and Fe, in the phase diagram it is assumed implicitly that an equilibrium nitriding potential is present as required for preventing decay.[7] Atomic nitrogen can be dissolved in α-Fe (bcc) to a concentration of about 0.4 at. % at 865 K. At concentrations higher than ~2.4 at. %, the bcc Fe lattice undergoes a tetragonal distortion, in which the N atoms randomly occupy octahedral hollow sites in the iron sublattice, forming the so-called N-martensite or α' phase. At the Fe_8N stoichiometry, the α' phase can transform, by heat treatments at low temperatures, into α''-$Fe_{16}N_2$, in which the N atoms are ordered.

When iron is in the austenite (γ, fcc) state (above 923 K) nitrogen can be dissolved to a maximum concentration of 10.3 at. %. The transformation of the iron sublattice from bcc to fcc takes also place when the γ'-Fe_4N phase, roaldite, is formed. Here the N atoms are placed in the body-centered position of the fcc iron sublattice. At even higher concentrations of N, the iron sublattice transforms into a hexagonal phase called ε, that can accept N in the concentration range from 25 at. % up to 33 at. %. The N atoms are randomly distributed in the octahedra formed by the Fe sublattice. At the Fe_2N stoichiometry, the ε phase can be transformed into ζ-Fe_2N, which has an orthorhombic structure, by ordering the N atoms over the octahedral sites. Although the phases at the nitrogen-rich side are less well known, recently the existence of two other cubic Fe-nitride phases has been reported with concentrations near 50 at. %.[8–11] The Fe sublattice in these phases is also fcc. According to theoretical calculations

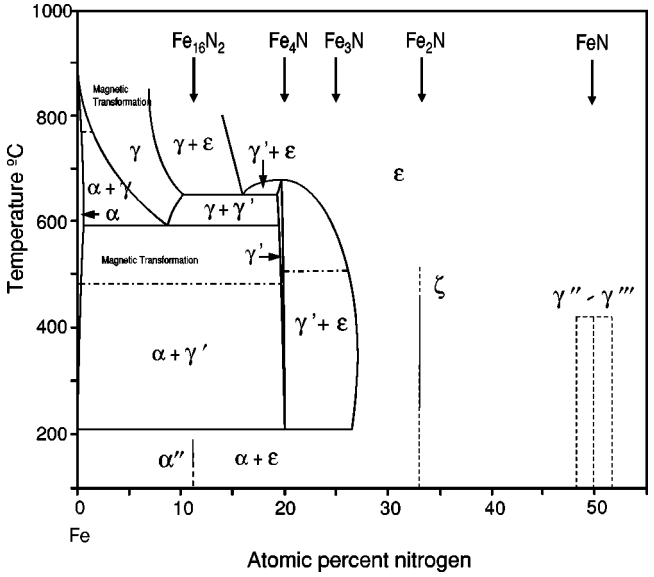

FIG. 1. Phase diagram of the Fe-N system.

two phases with the FeN stoichiometry can exist: γ''-FeN with a ZnS type of structure, and γ'''-FeN, with a NaCl type of structure.[12–16]

Most of the nitrides at the nitrogen-poor side of the phase diagram are ferromagnetic. Since the first report of its giant magnetic moment (with a saturation magnetization B_s of 2.8 T, as compared to 2.16 T for α-Fe),[17] α''-$Fe_{16}N_2$ has been the subject of many theoretical and experimental studies. The reported magnetic moments, however, show a wide scatter from 2.4 to 3.2 μ_B/Fe atom,[2] and no agreement has been reached regarding the giant moment. The main difficulty in determining the magnetic moment seems to be the inability to grow this phase in its pure form.

Following in importance (from the magnetic point of view) is γ'-Fe_4N. This is a magnetic conductor with a saturation magnetization of 1.8–1.9 T,[18] and a Curie temperature of 767 K. The magnetic properties of (100)-oriented films of pure γ'-Fe_4N epitaxially grown on MgO(100) have been recently reported.[19] It was found that the films have in-plane anisotropy with an anisotropy constant of $2.9\pm0.4\times10^4$ J/m^3. These and the other mentioned properties make γ'-Fe_4N a good candidate for applications as a magnetic layer in magnetic devices, as an alternative to Fe layers. Due to the Fe-N binding the intermixing problems with other components of the device, often encountered with Fe layers, may be reduced.

The magnetic moment of the ε phase decreases rapidly with increasing iron content and the Curie temperature changes from 535 K for Fe_3N (with a magnetic moment of $1.9\mu_B$) to 9 K for Fe_2N. The ζ-Fe_2N phase is possibly a very weak itinerant ferromagnet.[20] Regarding the cubic FeN phases, the γ'' ZnS-type nitride has been reported to be a nonmagnetic metal, and the γ''' NaCl-type an antiferromagnet,[20,21] but other possibilities have also been considered.[22]

As stated before, all these iron nitride phases are metastable with respect to decomposition into N_2 gas and α-Fe, although the kinetics of this process is quite slow at temperatures below 670 K (the actual decomposition temperature depends on the phase). At higher temperatures the decomposition can lead to the formation of voids filled with N_2. This metastability implies that the production of iron nitrides cannot be performed in N_2 gas. Nitridation in NH_3/H_2 gas mixtures is a well-established technique, by means of which one can control the production of one of the three main phases (α', γ', or ε) and transfer one phase to another, all according to the Lehrer diagram.[6,23] Other growth methods include reactive sputtering,[24] ion implantation,[25] or laser nitriding.[26] These methods give textured or multi-phase films.

Recently, molecular beam epitaxy (MBE) of Fe assisted with a source of atomic nitrogen was applied for the growth of different iron nitrides.[27,28] Epitaxial growth of α''-$Fe_{16}N_2$ (although no single-phase) on InGaAs-(001) (with or without an Fe buffer layer),[29] GaAs(001),[30] and MgO(001) (with an Fe buffer layer)[31] has been claimed. It has also been reported that the α'-Fe_8N and γ'-Fe_4N phases can be grown epitaxially on Si(001) using a Ag buffer layer by conventional reactive (N_2) dc magnetron sputtering.[32] α' can also grow epitaxially on GaAs(001) using Ag or Fe buffer layers by the sputter beam method.[33,34] Another method reported recently to produce epitaxial γ'-Fe_4N films on MgO(001) is by high-pressure chemical vapor deposition of NH_3 and $FeCl_3$.[35] In any of these studies, however, neither a detailed structure characterization (purity, crystalline quality, surface roughness) was performed nor the question of the atomistic mechanisms of growth was addressed.

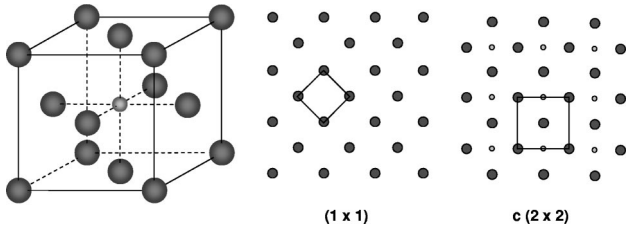

FIG. 2. (a) Unit cell of γ'-Fe_4N. The large, darker balls represent the Fe atoms, while the small, lighter ball represents the N atoms. (b) The two different types of planes along the [100] direction. The lines indicate the unit cell within the planes.

In the present paper the growth of epitaxial layers of γ'-Fe_4N is studied. This study is motivated not only by the potential for applications of such layers, but also by the prospect of revealing the main features of the growth mechanism of this compound, involving the reaction of a gas and a metal. This type of growth is often applied, for instance to obtain oxide layers. Although the recipes for the growth of such layers are well established, little is known about the mechanisms of the growth at the atomic scale.

In recent work of our group, high-quality epitaxial films of γ'-Fe_4N have been grown on MgO(100) by molecular beam epitaxy of iron in the presence of nitrogen obtained from a radio-frequency (rf) atomic source.[28,36,37] It was found that layers of high crystalline quality could be obtained at a low evaporation rate of Fe ($\sim$0.02 Å/s) in the presence of a gas flow containing atomic nitrogen and hydrogen. The best substrate temperature during growth for obtaining perfect layers was in the 600–670 K range. With the substrate at room temperature, no epitaxial layer growth was possible; a nanocrystalline or amorphous layer containing a mixture of nitrides was grown instead. No nitride was formed in case the substrate temperature was 730 K or more. A pure Fe layer was grown instead. The use of an insulating substrate, however, prevents the use of most of the standard *in-situ* surface science analysis techniques, and only rather thick films (100–300 Å) were analyzed, mostly *ex-situ*.

To avoid this problem, and trying to get a deeper insight into the mechanisms of growth, specially during the early stages, we have used a Cu single crystal, (100) oriented, as substrate. Bulk Cu has a fcc structure, with a lattice parameter $a=3.615$ Å. In γ'-Fe_4N the iron atoms form a fcc sublattice, while the nitrogen atom sits at the bcc position of the cubic cell, occupying one of the four octahedral hollow sites [Fig. 2(a)]. The lattice parameter is $a=3.795$ Å, so the misfit with the Cu lattice is 4.7%, and epitaxial grow should, in principle, be possible. We have previously reported a scanning tunneling microscopy (STM) study on the growth of quantum magnetic dots of γ'-Fe_4N on Cu(100).[38] In this paper, we extend that report to the growth and characteriza-

tion of high-quality, continuous iron nitride films. The results show that, under the appropriate growth conditions, high quality thin γ'-Fe_4N films, (100) oriented, can be grown layer by layer and epitaxially on Cu(100), with a sharp interface and a reduced surface roughness.

II. EXPERIMENT

The experiments were performed in an ion-pumped ultrahigh vacuum chamber (base pressure of 10^{-10} mbar) equipped with a home made STM unit and a rear-view four-grids low energy electron diffraction (LEED) optics, which was also used for Auger electron spectroscopy (AES). The substrate was a Cu(100) single crystal mechanically polished and cleaned by cycles of Ar^+ sputtering (500 eV) and annealing at 850 K until no contamination was present in the AES spectrum. The LEED pattern of this surface presented the expected (1×1) four-fold symmetry characteristic of the (100) face of an fcc substrate.

The iron nitride films were grown by depositing iron from a home-made electron gun in the presence of a flux of atomic nitrogen obtained from a radio-frequency (rf) plasma source.[37] The rf source was used with a mixture of nitrogen and hydrogen (in a ratio of 1:1) for a total pressure of 10^{-2} mbar. The applied power was 60 W. A retractable tube, coated on the inside with Teflon to reduce the recombination of N atoms, was used to direct the gas from the plasma container to the sample. During growth, the substrate temperature was 670 K. From earlier work we know that these conditions result in the growth of epitaxial γ'-Fe_4N films on MgO(100) substrates.[28,36,37]

The Fe deposition rate was measured by independently calibrating the Fe evaporator (with no nitrogen over the sample) by means of STM images (for submonolayer coverages) and AES spectra (for larger coverages). The coverages given in this paper for the nitride films where obtained from the AES spectra or just by measuring the deposition time (when no AES signal of the deposited Fe could be detected) and are then referred to as the equivalent amount of Fe on the substrate, with an estimated error around 20%.

III. RESULTS

A. Separated deposition of Fe and N

The growth of iron nitrides on Cu(100) is a complex process, where different species (Fe, N, N_2, H, and H_2) are arriving at a surface held at high temperature (670 K). This gives rise to a large set of competing atomistic processes (surface diffusion, exchange processes, binding, dissociation, reaction, etc.), whose interplay makes it very difficult to identify the relevant growth mechanisms. Trying to separate the different contributions, we have carried out experiments where, in one case, Fe was deposited at 670 K on Cu(100) (with no flux of N present), and in the second case, the Cu surface, held at 670 K, was exposed exclusively to a flux of N atoms coming from the rf source.

1. The high temperature growth of Fe on Cu(100)

Although the Fe/Cu(100) system has been thoroughly studied, mainly due to the possibility of stabilize epitaxial films of fcc Fe and study their magnetic properties, almost all the studies have been carried out after depositing Fe on a Cu substrate held at room- or lower temperatures. Since the surface free energy of Fe (2.9 Jm^{-2}) is significantly larger than the surface energy of Cu (1.9 Jm^{-2}), the Fe-on-Cu system is metastable, and Cu has a strong tendency to segregate to the surface.[39–41] For deposited films, the onset temperature for this process depends on the film thickness, and varies from room temperature for submonolayer films to ~650 K for thicker films.[39] Thus, deposition at high temperatures unavoidably would result in strong intermixing.

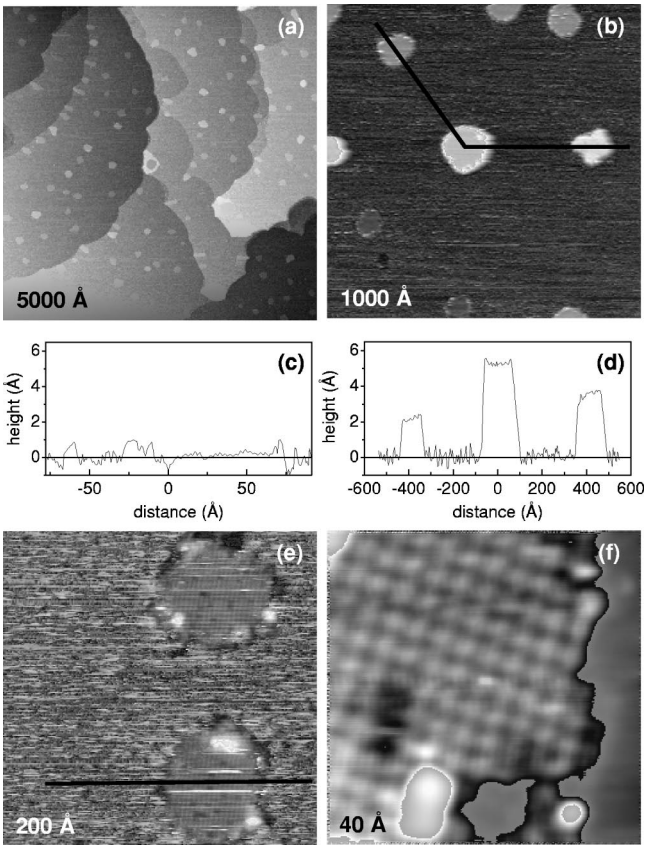

FIG. 3. STM images taken at 300 K after depositing 0.3 ML of Fe on Cu(100) at 670 K. The graphs in (c) and (d) represent height profiles taken along the lines drawn in (e) and (b), respectively. (f) shows an atomic resolution image of one of the islands.

Figure 3 shows some STM images taken after depositing 0.3 ML of Fe with the Cu substrate held at 670 K. Circular islands with a density $7\times10^{10}/cm^2$ appear at the surface. The average lateral size of the islands is 100 Å, while they seem to be one (~1.9 Å), two (~3.6 Å) or three (~5.1 Å) levels high, as shown in the profile plot in Fig. 3(d). There are also some features, with the same structure as the islands, but embedded within the substrate surface [see Fig. 3(e), and the line profile in Fig. 3(c)]. The top of the islands is atomically flat, and a square array of atoms, with a 3.6 Å $\times$3.6 Å (±0.1 Å) unit cell can be seen on some of them [Fig. 3(f)], which is consistent with the (weak) $c(2\times2)$ LEED pattern visible at this stage of growth. Since no Fe signal can be detected with AES, the surface of the islands must be composed of Cu [the attenuation length of the low

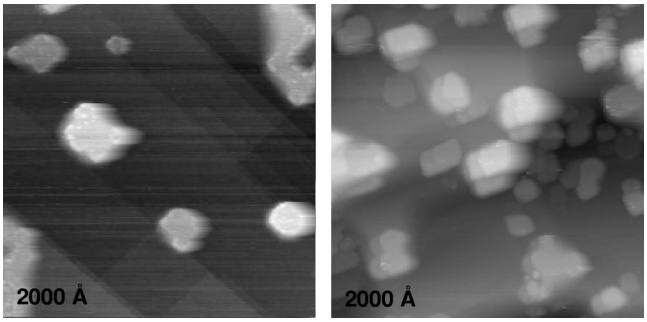

FIG. 4. STM images taken after depositing 0.8 (left) and 1.2 (right) MLs of Fe on Cu(100) at 670 K.

energy Auger transition of Fe (47 eV) is around ~2 atomic layers].[42] It is noteworthy, however, that such islands would not be stable on a clean Cu surface after heating at 670 K, implying that they must be stabilized by buried Fe. Since the mixing energy for the Fe-Cu system is positive,[43] Fe and Cu will not form binary alloys and the two metals will not mix. Thus we conclude that the deposited Fe forms two-dimensional (2D) islands [or maybe three-dimensional (3D) clusters] buried below the top Cu surface, but not too far away, since it does affect the Cu surface on top, inducing a $c(2\times2)$ reconstruction.

When the amount of Fe deposited is around 1 ML (Fig. 4), the lateral size of the islands increases slightly, but more dramatically, their height now ranges between 10 and 50 Å. Since only the Cu signal can be detected with AES, and the LEED has reverted to the original (1×1), we conclude that the deposition of a small amount of Fe at 670 K has caused a considerable amount of Cu to appear on the surface. After depositing ~8 MLs of Fe, a small Fe AES signal could be detected, but at this stage the surface was rather rough and facetted.

2. Adsorption of N on Cu(100) at high temperature

The adsorption of N on Cu has also been studied. Although molecular nitrogen does not adsorb on Cu surfaces, up to half a monolayer of N atoms can be adsorbed at 300 K on Cu(100) if the gas is atomized by using an ion or an electron gun.[44,45] After annealing at 670 K, the disordered N overlayer thus created orders in a $c(2\times2)$ pattern. For low coverages this $c(2\times2)$ overlayer is self-organized in a lateral array of square-shaped islands, with sides ~52 Å long, separated by several rows of bare Cu.[46] This self-organized surface has been used as a template for the fabrication of arrays of metallic magnetic nanostructures.[47]

In our case, the surface was held at 670 K during exposure, and the atomic N was produced by the rf plasma source. Figure 5 shows a representative STM image taken at 300 K after exposing the Cu surface for 8 minutes to the flux of nitrogen (plus hydrogen, although at this high deposition temperature hydrogen is not expected to stick to the Cu surface).[48] Although the LEED pattern was similar to the one of the clean Cu surface, Auger electron spectroscopy did detect the presence of N and no other signal besides Cu, so it is reasonable to assume that the dark features visible on the surface, with an apparent depth around 0.7 Å, are N atoms. A similar pattern of dark patches has been reported for N on Fe(100).[49] Actually, the N atoms are expected to be imaged as depressions on flat metallic surfaces.[50,51] Figure 5 shows that the steps of the original surface appear decorated by N atoms. The N atoms can be found both isolated, or forming clusters with a minimum separation of ~3.6 Å. This corresponds to the next-nearest-neighbor distance, and thus to a local $c(2\times2)$ reconstruction. Clusters with a crosslike shape are often seen, indicating that this structure is relatively stable.

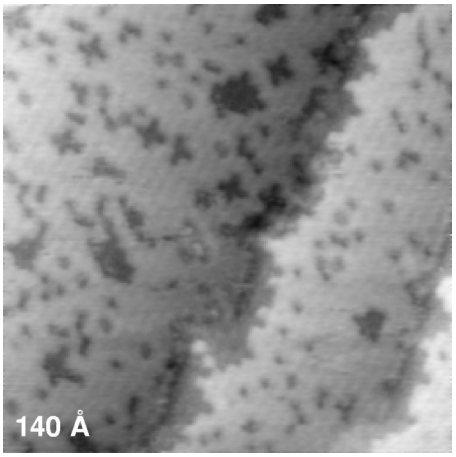

FIG. 5. STM image (140 Å×140 Å) taken after exposing for 8 minutes the Cu surface, held at 670 K, to the flux of atomic N coming from the rf plasma source. The sample bias voltage was 0.44 V.

Figure 6 shows two images of the same surface region recorded with an interval of 90 s. The configuration of some of the N atoms changes from one frame to another, demonstrating that N diffuses on Cu(100) even at room temperature. Making an analysis similar to that in Ref. 49, the diffusion barrier for isolated atoms can be estimated to be 0.88 ± 0.05 eV. This number is to be compared with the measured diffusion barrier for isolated N adatoms on Ru(0001) ×(0.94 eV) (Ref. 52) or Fe(100) (0.92 eV).[49] This implies that at the growth temperature of the iron nitride films (670 K), the N atoms must be very mobile.

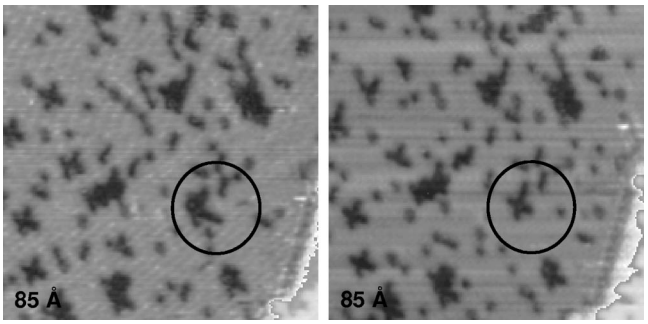

FIG. 6. Two STM images (85 Å×85 Å) of the same region of the Cu(100) surface after exposure to the flux of atomic nitrogen. They are taken with a time interval of 90 s.

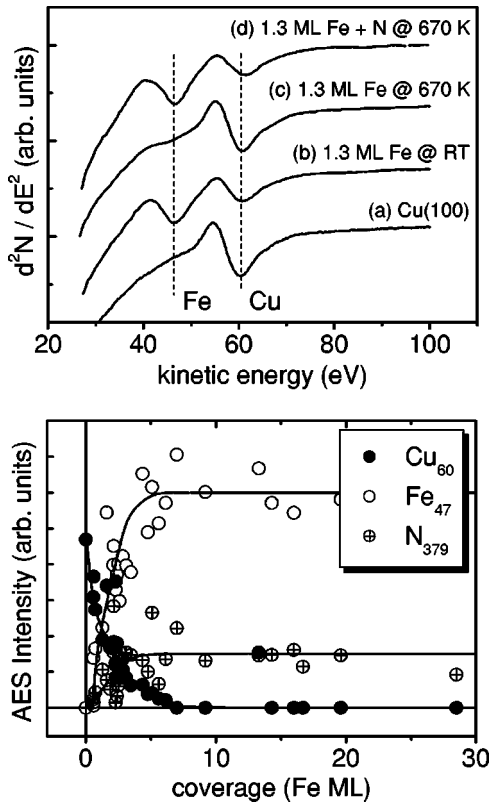

FIG. 7. Top panel, low energy part of the Auger spectra taken (a) on the clean Cu(100) surface, and after depositing 1.3 ML of Fe with the Cu substrate, (b) at room temperature; (c) at 670 K; and (d) at 670 K in the presence of the flux of atomic nitrogen. Bottom panel, evolution of the intensities of the Fe_{47}, Cu_{60}, and N_{379} Auger transitions as a function of the thickness of the nitride layer.

B. Nitride films

1. Reduction of the Fe-Cu intermixing

As we have seen above, deposition of Fe on Cu at high temperature unavoidably leads to substantial Cu segregation and intermixing. This is *not* the case when atomic N is simultaneously arriving to the surface. The presence of N reduces considerably the amount of Fe-Cu intermixing, even at high temperature. The top panel in Fig. 7 shows the low-energy part of the Auger spectra taken from the clean Cu surface, and after depositing ~1.3 ML of Fe under three different conditions. For this coverage, when Fe is deposited at room temperature [curve (b)], the Auger signals corresponding to the Fe MVV Auger transition (47 eV) and the Cu MVV transition (60 eV) have approximately the same intensity. At 670 K [curve (c)], as a consequence of the strong intermixing between the deposited Fe and the Cu substrate, the signal corresponding to Fe is barely discernible. This indicates that all the material close to the surface is Cu (see Fig. 4), the deposited Fe being buried deep into the substrate. However, when N is present [curve (d)], the intensities of the Auger signals are almost identical to those at 300 K, thus proving that the codeposition with N has reduced (almost) completely the segregation of Cu to cover the deposited Fe.

This is further confirmed by measuring the evolution of the intensities of the Fe_{47}, Cu_{60}, and N_{379} Auger transitions as a function of the amount of Fe deposited, as shown in the bottom panel of Fig. 7. The Cu signal coming from the substrate decreases quickly with the film thickness, and after depositing 5–6 ML of Fe+N it has almost completely disappeared. This is consistent with a layer by layer type of growth, with little, if any, interdiffusion between the deposited Fe and the Cu substrate. Thus, the presence of N efficiently prevents the segregation of Cu to the surface, probably by reducing the surface free energy of the growing film. At the same time, the intensities of the Fe and N signals increase initially very quickly and, approximately for the same coverage (~5 ML), they reach stable values, which indicates the formation of an stoichiometric Fe-N compound for thicker films. We shall see below that this compound is γ'-Fe_4N.

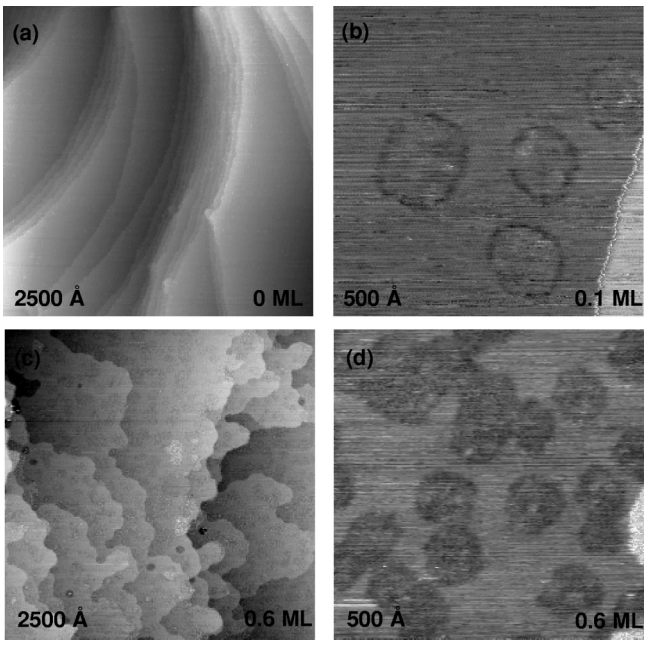

FIG. 8. STM images of (a) clean Cu(100); and after depositing (b) ~0.1 MLs; (c) and (d) 0.6 MLs of Fe+N at 670 K.

2. The early stages

Figure 8(a) shows a large-scale STM image of the clean Cu(100) surface, where monoatomic steps separating large terraces (several hundreds of Ångstroms wide) can be seen. After depositing submonolayer quantities of Fe in the presence of the flux of N at 670 K, a certain number of dark, almost circular patches (with an average diameter close to 100 Å) appears on the STM images [Fig. 8(b)]. At this point, the morphology is similar to the one resulting from depositing pure Fe, and even the size of the patches is similar to the size of the islands formed when no N is present (compare to Fig. 3), but now the AES spectra demonstrate clearly the presence of *both* Fe and N in the surface, while the Cu signal coming from the substrate is still clearly visible. When increasing the deposition time the density of patches increases, while their size remains approximately constant [Figs. 8(b)–8(d)]. Otherwise the surface of the terraces seems unaffected (no sign of foreign inclusions can be detected), so

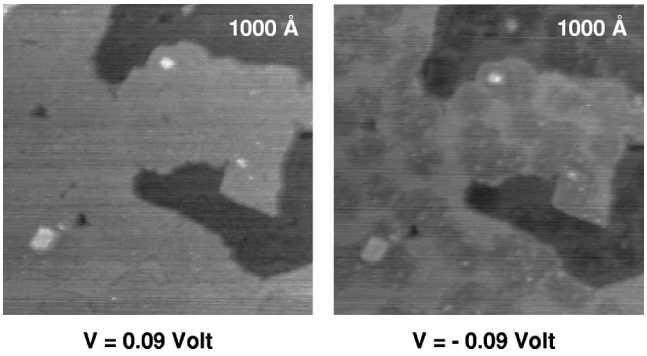

FIG. 9. Two STM images of the same area of the Cu surface after depositing a small amount of Fe+N at 670 K, taken with different sample bias voltages.

we conclude that these patches must be composed of both Fe and N. Thus the area between the patches consists of pure Cu.

The aspect of these patches, and their apparent height with respect to the surrounding Cu terraces, depend drastically on the tunneling parameters. Figure 9 reproduces two images of the same area of the surface taken with different bias voltages. While in one case the patches can hardly be distinguished, in the second case their apparent height is ~0.6 Å below the surface layer. This confirms that the patches have a different electronic structure, and therefore a different chemical composition than the surrounding terraces.

It can be concluded that the patches are islands with an iron nitride composition that are embedded within the topmost surface layer of the Cu substrate. A further point supporting this conclusion is the change in the shape of the steps of the Cu substrate after deposition. While in Fig. 8(a) the steps look regular, homogenous, and straight on a short scale, in Fig. 8(c) the steps are more irregular and rounded, indicating a noticeable amount of transport of substrate atoms over the surface. This points to an exchange process between the incoming Fe atoms and the Cu atoms at the surface.[53] The Cu adatoms thus created will accumulate at step edges. Step rounding after metal deposition has been frequently observed,[54–59] and it was always associated with intermixing between the deposited atoms and the substrate atoms by an exchange mechanism.

Similarly to other metal on metal systems [e.g., Co/Cu(100) or Fe/Au(100) around 300 K],[53,60,61] the exchange process between the deposited Fe and the Cu substrate is strongly reduced before the original surface is completely covered by the embedded islands. The ejected Cu atoms (plus those originated from the steps of the initial Cu surface) nucleate islands on the terraces, where the process of exchange with Fe, formation of embedded Fe islands and decoration of the islands by N is repeated, though at a reduced scale.

Figure 10 shows a large STM image recorded on a 1.6 ML thick nitride film. At this stage the film is very flat, showing essentially two levels: the original substrate surface (with the embedded nitride islands), and a more than half completed first layer (there is a small percentage of second level islands). The connected nature of the first layer islands indicates a large diffusion coefficient of all its constituents. The first layer, however (see the lower right part of Fig. 10), is not chemically homogeneous. Changing the bias voltage allows to visualize again islands embedded on it. The contrast seen in the original surface layer (mainly chemical, but partly structural) is due to the inclusion of the nitride islands, as mentioned above. In some cases it has been observed that this contrast is transferred to the second layer. Films thicker than 3 ML do not show the chemical contrast reported here for the original surface and the first deposited layer. Thus, the presence of N limits the intermixing reaction between Fe and Cu at 670 K to the first two layers, further quantifying the AES observations described above.

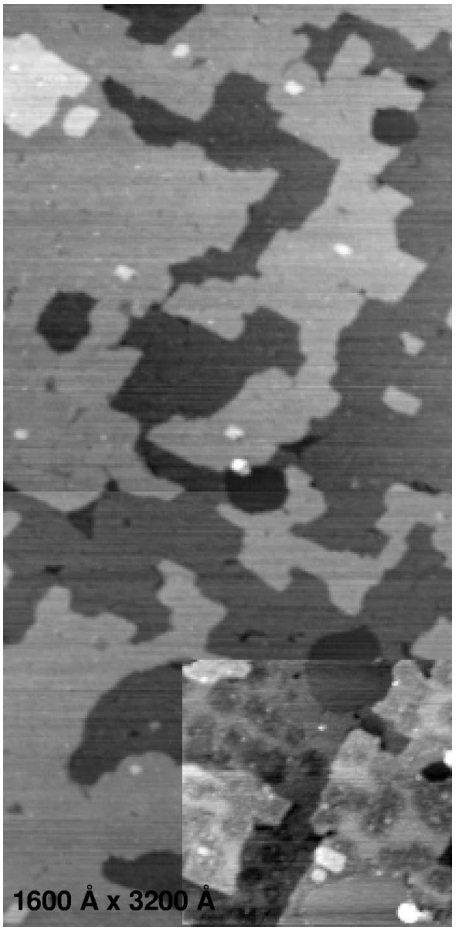

FIG. 10. STM images taken after depositing 1.6 MLs of Fe +N on Cu(100) at 670 K. The lower right part of the image was taken with a different bias voltage.

C. Thick films. Phase identification and magnetic properties

After the initial transient, the films grow layer by layer. Figure 11 shows three large scale STM images taken on films 9.2, 13.3, and 270 ML thick. All these films were chemically homogeneous as seen by STM. Besides some dislocations, a few holes, and a number of square or rectangular islands, the films present a rather flat growth front, with only 3–4 levels exposed, as can be seen in the height profile in

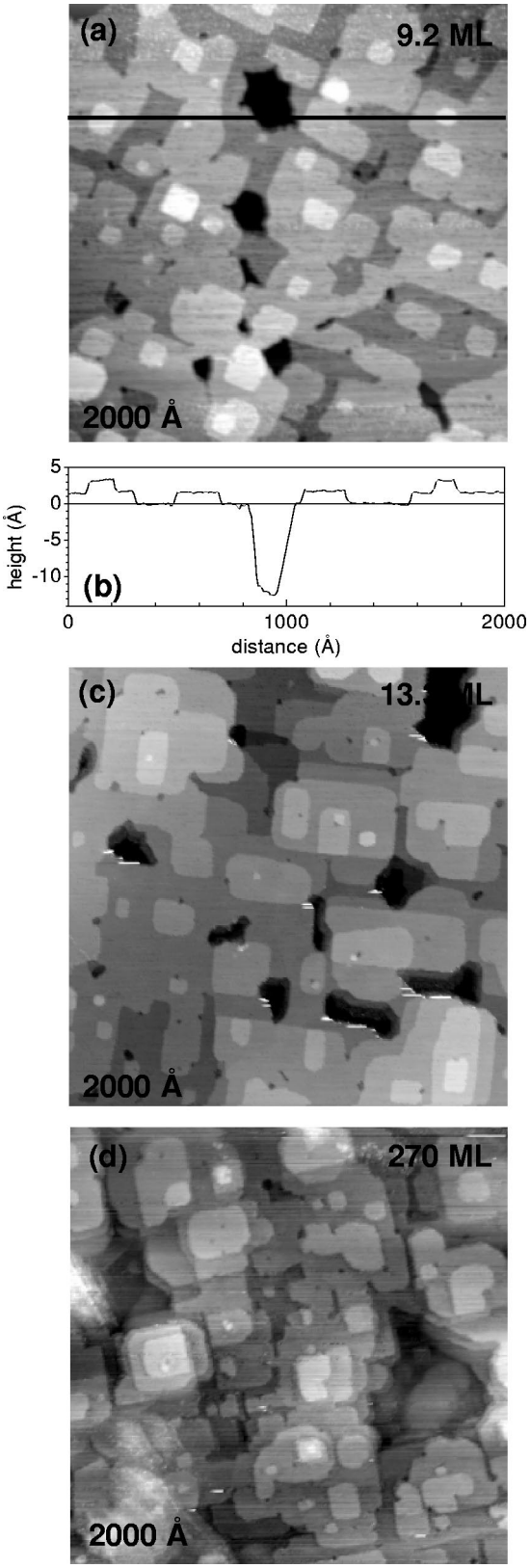

FIG. 11. STM images (2000 Å×2000 Å) taken after depositing (a) 9.2, (c) 13.3, and (d) 270 MLs of Fe+N on Cu(100) at 670 K. The graph in (b) represents the height profile along the line drawn in (a).

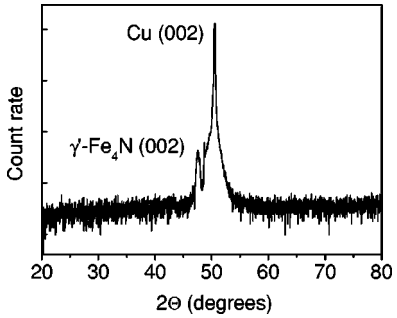

FIG. 12. X-ray diffraction scan taken on a iron nitride film ~200 Å thick grown on Cu(100).

Fig. 11(b). Even after depositing 270 MLs of iron nitride [Fig. 11(d)], a smooth surface is still clearly visible. Such a small roughness is rarely encountered when growing metallic films by thermal deposition. Note that at every stage there are holes, which size increases with their depth from a few Ångstroms to hundreds of Ångstroms. Their apparent depth (limited by the tip shape) can be up to 20 Å, and for the thinner films they probably reach down to the initial Cu surface. Thus it seems that holes, the main visible type of defect in the growing film, are continuously created at every layer, perhaps because the chosen deposition temperature was too close to the decomposition temperature of the iron nitride.

As mentioned before, when increasing the deposition time the Auger signals from N and Fe reach stationary values, which seems to indicate the formation of an stoichiometric Fe-N compound, independent of the film thickness. X-ray diffraction (XRD) and conversion electron Mössbauer (CEMS) spectroscopy taken on thicker films grown under identical conditions (although in a different system) show that the compound formed is pure, single phase, γ'-Fe_4N.

Figure 12 shows the x-ray diffractogram in the $\theta-2\theta$ geometry, taken *ex-situ* on a film ~200 Å thick. The only peaks visible can be assigned to the (002) reflection from the Cu substrate and the (002) reflection from γ'-Fe_4N. From this and other out-of-plane scans (not shown) the in-plane and out-of-plane lattice parameters can be calculated. It turns out that, for this thickness, the Fe_4N is still slightly tetragonally distorted, with $a=3.781$ Å(-0.37%) and $c=3.806$ Å $(+0.29\%)$. The epitaxial relationship between the nitride film and the Cu substrate is

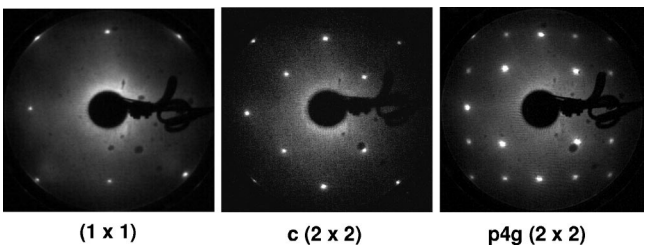

FIG. 13. LEED patterns taken on (a) the clean Cu(100) surface; (b) and (c) the iron nitride thin films, at an energy of 110 eV.

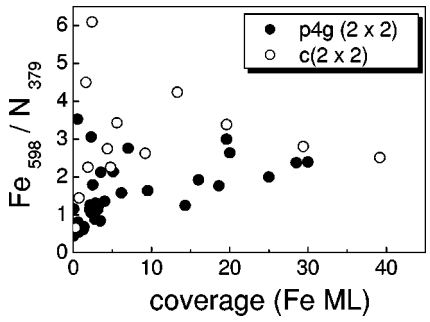

FIG. 14. Intensity ratio between the Fe and N Auger signals for iron nitride films. Full circles correspond to films displaying a p4g(2×2) LEED pattern, and empty circles to films showing a c(2×2) LEED pattern.

$$[100]_{\gamma'} \| [100]_{\mathrm{Cu}},$$
$$(001)_{\gamma'} \| (001)_{\mathrm{Cu}}. \tag{1}$$

In the [100] direction, γ'-Fe_4N can be viewed as composed of alternating planes with two different compositions. The first one [Fig. 2(b)], is composed exclusively of Fe atoms forming a square arrangement whit a unit cell size of $d_{Fe_4N}=2.683$ Å. Since the size of the Cu(100) surface unit cell is $d_{Cu}=2.556$ Å, this structure would produce a (1×1) LEED pattern. The second type of plane [Fig. 2(c)] contains both Fe and N atoms, and the surface unit cell can be described as a $(\sqrt{2}\times\sqrt{2})$R45°, also known as c(2×2), with respect to the Cu surface unit cell.

From the very early stages of growth, all the grown films (up to a thicknesses of 300 Å), displayed either a c(2×2) LEED pattern [Fig. 13(b)], or the closely related p4g(2×2) pattern [Fig. 13(c)].[48,62–65] The two LEED patterns correspond to different surface terminations of the nitride films. Figure 14 shows the ratio of the Fe_{598} and the N_{379} Auger signals, as a function of the thickness of the nitride layers. The value of this ratio is somewhat larger for those films displaying a c(2×2) LEED pattern. This suggests that the different LEED patterns are correlated with a different relative amount of N at the surface. In fact, the LEED pattern could be modified at will by depositing small amounts of Fe or N on the grown films. If a 40 Å nitride film displaying a c(2×2) LEED pattern film (and with Auger intensity ratio $Fe_{598}/N_{379}=3.4$), was exposed at 670 K for five minutes to a flux of atomic N, the LEED pattern changed to a p4g(2×2) symmetry (while the AES ratio decreased to $Fe_{598}/N_{379}=1.8$). If 2 ML of Fe are deposited at 300 K on top of this film, the LEED pattern reverts to the original c(2×2) (and the ratio Fe_{598}/N_{379} increases to 2.47). Thus it seems clear than the p4g(2×2) and the c(2×2) LEED patterns correspond to different surface terminations of a γ'-Fe_4N-(100) oriented nitride film, with the p4g(2×2) having a larger N concentration in the region probed by AES.

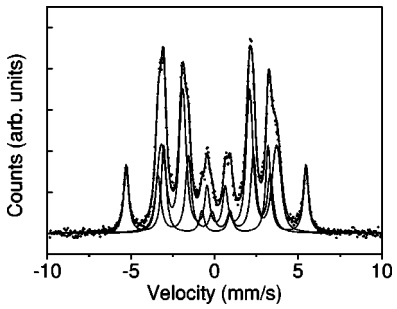

FIG. 15. CEMS spectrum taken ex-situ on a γ'-Fe_4N film ~200 Å thick.

A p4g(2×2) LEED pattern has been observed in some adsorbate systems, like N on Ni(100).[63] In this reconstruction the adsorbate atoms, that form a c(2×2) overlayer structure, are sitting in hollow sites almost at the same level than the surface atoms, while the four substrate atoms surrounding each adsorbate rotate clockwise or counterclockwise. In a similar way, a possible structure for the p4g(2×2) reconstruction would be the adsorption of an *extra* N overlayer on an Fe-only terminated plane of the nitride film, while a simple Fe-N termination of the bulk would give the c(2×2) LEED pattern. This would explain the larger value of the Fe/N ratio for the c(2×2) termination.

The conversion electron Mössbauer spectroscopy (CEMS) spectrum of a 250 Å film is shown in Fig. 15. There are two non-equivalent crystallographic sites of the iron atoms in the unit cell of γ'-Fe_4N, which are the cubic corner (Fe^{I}) and the face-centered (Fe^{II}) sites. Because the easy magnetization is parallel to the ⟨100⟩ direction, the Mössbauer subspectrum for the Fe II site is split into two additional subspectra with an intensity ratio of 2:1. Therefore, the whole spectrum can be fitted to three sextets with an intensity ratio $Fe^{I}:Fe^{II}_{A}:Fe^{II}_{B}=1:2:1$,[66] plus a small (4%) nonmagnetic component. The results of the fit are given in Table I, together with the generally accepted values (taken from

TABLE I. Mössbauer parameters (RA is Relative area; IS is Isomer shift; HF is hyperfine field; QS is quadrupole splitting) obtained from the analysis of the CEMS data for a 250 Å iron nitride film grown on Cu(100). The values in parentheses are taken from Ref. 66.

	RA %	IS mm/s	HF I	QS mm/s
γ' Fe^{I}	24	0.094 (0.24)	33.27 (34.06)	+0.01 (0.0)
γ' Fe^{II}_{A}	48	0.185 (0.30)	21.32 (21.55)	+0.17 (+0.22)
γ' Fe^{II}_{B}	24	0.184 (0.32)	20.76 (21.92)	−0.40 (−0.43)
	4	0.266		+1.39

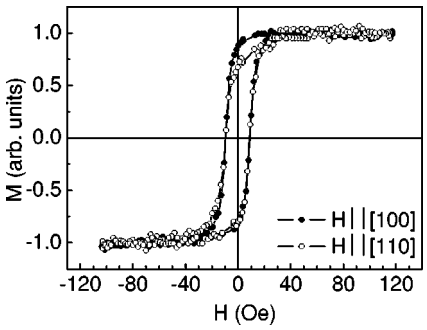

FIG. 16. In-plane magnetic hysteresis loops for a 300 Å thick iron nitride film recorded at 300 K along two different directions.

Ref. 66). Although the fit is quite good, the values of the hyperfine fields are slightly smaller. The width of the peaks ($\sim$0.40 mm/s) is larger than for similar samples grown on MgO substrates ($\sim$0.25 mm/s).[67] These two facts may indicate a higher degree of disorder in the films grown on Cu(100).

The magnetic properties of the nitride films at 300 K have been determined *ex-situ* by using surface magneto-optic Kerr effect. The easy axis of magnetization lies in the film plane, and is parallel to the <100> direction, as in bulk γ'-Fe_4N.[66] Two in-plane hysteresis loops for a 300 Å thick nitride film measured along the main crystallographic directions are shown in Fig. 16. The coercivities are rather low, around 10 Oe, in both cases.

IV. DISCUSSION

We have shown that high-quality iron nitride films can be grown epitaxially on Cu(100) by MBE of Fe assisted by an atomic nitrogen plasma source. The growth starts with the formation of iron nitride islands embedded within the top surface Cu layer. It is conceivable that these islands are initially created by exchange of the Fe atoms with the substrate Cu atoms. Adsorption of an Fe atom in or below the surface is energetically favorable over adsorption on the surface[68] and the exchange process (in the absence of N) has been observed already at 300 K.[69] At the growth temperature of 670 K the mobility of the Fe atoms is very high, and they tend to cluster.[43,68] This mechanism seems to be valid both with and without N. In the second case, however, the Fe islands prefer to be covered by Cu atoms, since the surface free energy of Cu(100) is lower than the surface free energy of Fe(100). This is not the case when N is present. The N atoms, which have a higher affinity to bond with Fe than with Cu, stick to the Fe islands, forming an iron nitride compound. Although, to our knowledge, there are no data of the surface free energies of the different iron nitrides, the surface energy of this compound is probably lower than the Cu one. This would explain why the nitride islands remain uncovered by Cu. As a consequence, the intermixing between the growing film and the Cu substrate is limited to the first monolayers.

After the initial stages, the nitride formed can be identified as γ'-Fe_4N, which grows layer by layer and epitaxially up to high thicknesses (hundreds of Ångstroms), with $[100]_{\gamma'}\|[100]_{Cu}$. It has been previously reported that, in general, the substrate temperature is very important to determine which phase is stable. Deposition at high temperatures [28,35,70–72] (or post-annealing of room temperature deposited phases)[73–75] favors the formation of γ'-Fe_4N over the other iron nitrides. γ'-Fe_4N has been reported to form at 370 K on Ag/Si(100) by reactive sputtering,[32] at 420 K on Si and GaAs by ion-beam enhanced deposition,[72] at 470 K on glass plates by ion-beam-assisted deposition,[71] between 470 and 670 K on MgO(100) by using gas-flow assisted MBE,[28,36] and at 870 K on MgO(100) by atmospheric pressure halide chemical vapor deposition.[35]

Thus, within the growth conditions, a substrate temperature of 670 K assures the formation of crystalline, single-phase γ'-Fe_4N. However, since nitrogen desorption becomes considerable at temperatures >700 K, some nitride decomposition cannot be neglected, which could originate the holes visible in the films. Homoepitaxial growth of Fe on bcc Fe(100) at 520 K occurs layer-by-layer.[76] The surface diffusion coefficient was given by $D=D_0e^{(-E/kT)}$, with $D_0=7.2\times10^{-8}$ m^2 s^{-1} and $E=0.45$ eV. For the diffusion coefficient of N in bulk γ'-Fe_4N, different values have been reported, with activation barriers ranging between 0.66 and 0.97 eV.[77–81] For N in α-Fe, activation barriers around 0.79 eV have been measured.[26,82,83] In any case, it can be safely assumed that the mobility of N atoms within the Fe matrix is rather large at the growth temperature. Under these conditions, it is tempting to consider the growth of Fe_4N as similar to the layer by layer, epitaxial growth of (fcc) Fe on Fe at high temperatures, with N atoms simultaneously seeking their way into the Fe lattice to form the most stable compound (γ'-Fe_4N) under these growth conditions.

ACKNOWLEDGMENTS

This work has been supported by the Spanish CICyT (under Grant No. MAT2001-0082-C04-02) and DGI (under Grant No. BFM2001-0174), and FOM.

[1] *Encyclopedia of Materials Science and Engineering*, edited by Michael B. Bever (Pergamon, United Kingdom, 1986), Vol. 4, p. 3210.

[2] J. M.D. Coey and P. A.I. Smith, J. Magn. Magn. Mater. **200**, 405 (1999).

[3] O. Kohmoto, IEEE Trans. Magn. **27**, 3640 (1991).

[4] A. R. Chezan, C. B. Craus, N. G. Chechenin, T. Vystavel, J. Th. M. de Hosson, L. Niesen, and D. O. Boerma, IEEE Trans. Magn. **38**, 3144 (2002).

[5] K. H. Jack, Proc. R. Soc. London, Ser. A **208**, 200 (1951).

[6] E. H. du Marchie van Voorthuysen, N. C. Chechenin, and D. O. Boerma, Metall. Mater. Trans. A **33A**, 2593 (2002).

[7] B. J. Kooi, M. A. J. Somers, and E. J. Mittemeijer, Metall. Mater. Trans. A **27**, 1063 (1996).
[8] N. Heiman and N. S. Kazama, J. Appl. Phys. **52**, 3562 (1981).
[9] A. Oueldennaoua, E. Bauer-Grosse, M. Foos, and C. Frantz, Scr. Metall. **19**, 1503 (1985).
[10] H. Nakagawa, S. Nasu, H. Fujii, M. Takahashi, and F. Kanamaru, Hyperfine Interact. **69**, 455 (1991).
[11] K. Suzuki, H. Morita, T. Kaneko, H. Yoshida, and H. Fujimori, J. Alloys Compd. **201**, 11 (1993).
[12] H. Shimizu, M. Shirai, and N. Suzuki, Physica B **237–238**, 546 (1997).
[13] H. Shimizu, M. Shirai, and N. Suzuki, J. Phys. Soc. Jpn. **66**, 3147 (1997).
[14] H. Shimizu, M. Shirai, and N. Suzuki, J. Phys. Soc. Jpn. **67**, 922 (1988).
[15] A. Filippetti and W. E. Pickett, Phys. Rev. B **59**, 8397 (1999).
[16] Y. Kong, J. Phys.: Condens. Matter **12**, 4161 (2000).
[17] T. K. Kim and M. Takahashi, Appl. Phys. Lett. **20**, 492 (1972).
[18] J. Q. Xiao and C. L. Chien, Appl. Phys. Lett. **64**, 384 (1994).
[19] J. L. Costa-Krämer, D. M. Borsa, J. M. García-Martín, M. S. Martín-González, D. O. Boerma, and F. Briones, Phys. Rev. B **69**, 144402 (2004).
[20] T. Hinomura and S. Nasu, Hyperfine Interact. **111**, 221 (1998).
[21] T. Hinomura and S. Nasu, Physica B **237–238**, 557 (1997).
[22] D. M. Borsa and D. O. Boerma (private communication).
[23] E. Lehrer, Z. Elektrochem. Angew. Phys. Chem. **36**, 383 (1930).
[24] A. Kano, N. S. Kazama, and H. Fujimori, J. Appl. Phys. **53**, 8332 (1982).
[25] A. M. Vredenberg, C. M. Prez-Martn, J. S. Custer, D. O. Boerma, L. de Wit, F. W. Saris, N. M. van der Pers, T. H. de Keijser, and E. J. Mittemeijer, J. Mater. Res. **7**, 2689 (1992).
[26] P. Schaaf, Prog. Mater. Sci. **47**, 1 (2002).
[27] M. Komuro, Y. Kozono, M. Hanazono, and Y. Sugita, J. Appl. Phys. **67**, 5126 (1990).
[28] S. Grachev, D. M. Borsa, S. Vongtragool, and D. O. Boerma, Surf. Sci. **482–485**, 802 (2001).
[29] Y. Sugita, K. Mitsuoka, M. Komuro, H. Hoshiya, Y. Kozono, and M. Hanazono, J. Appl. Phys. **70**, 5977 (1991).
[30] Y. Sugita, H. Takahashi, M. Komuro, M. Igarashi, R. Imura, and T. Kambe, J. Appl. Phys. **79**, 5576 (1996).
[31] C. Ortiz, G. Dumpich, and A. H. Morrish, Appl. Phys. Lett. **65**, 2737 (1994).
[32] M. A. Brewer, K. M. Krishnan, and C. Ortiz, J. Appl. Phys. **79**, 5321 (1996).
[33] S. Okamoto, O. Kitakami, and Y. Shimoda, J. Appl. Phys. **79**, 1678 (1996).
[34] S. Okamoto, O. Kitakami, and Y. Shimada, J. Appl. Phys. **79**, 5250 (1996).
[35] N. Takahashi, Y. Toda, T. Nakamura, and T. Fujii, Jpn. J. Appl. Phys., Part 1 **38**, 6031 (1999).
[36] D. M. Borsa, S. Grachev, D. O. Boerma, and J. W. K. Kerssemakers, Appl. Phys. Lett. **79**, 994 (2001).
[37] S. Yu. Grachev, D. M. Borsa, and D. O. Boerma, Surf. Sci. **516**, 159 (2002).
[38] J. M. Gallego, S. Yu Grachev, M. C.G. Passeggi, Jr., F. Sacharowitz, D. Ecija, R. Miranda, and D. O. Boerma, Phys. Rev. B **69**, 121404 (2004).
[39] Th. Detzel and N. Memmel, Phys. Rev. B **49**, 5599 (1994).
[40] N. Memmel and Th. Detzel, Surf. Sci. **307–309**, 490 (1994).
[41] J. Shen, J. Giergiel, A. K. Schmid, and J. Kirschner, Surf. Sci. **328**, 32 (1995).
[42] M. P. Seah and W. A. Dench, Surf. Interface Anal. **1**, 2 (1979).
[43] A. Christensen, A. V. Ruban, P. Stoltze, K. W. Jacobsen, H. L. Skriver, J. K. Norskov, and F. Besenbacher, Phys. Rev. B **56**, 5822 (1997).
[44] R. N. Lee and H. E. Farnsworth, Surf. Sci. **3**, 461 (1965).
[45] G. G. Tibbetts, J. M. Burkstrand, and J. C. Tracy, Phys. Rev. B **15**, 3652 (1977).
[46] F. M. Leibsle, C. F. J. Flipse, and A. W. Robinson, Phys. Rev. B **47**, 15865 (1993).
[47] T. M. Parker, L. K. Wilson, N. G. Condon, and F. M. Leibsle, Phys. Rev. B **56**, 6458 (1997).
[48] I. Chorkendorff and P. B. Rasmussen, Surf. Sci. **248**, 35 (1991).
[49] M. Ø. Pedersen, L. Österlund, J. J. Mortensen, M. Mavrikakis, L. B. Hansen, I. Stensgaard, E. Lægsgaard, J. K. Nørskov, and F. Besenbacher, Phys. Rev. Lett. **84**, 4898 (2000).
[50] P. Sautet, Surf. Sci. **374**, 406 (1997).
[51] I. S. Tilinin, M. K. Rose, J. C. Dunphy, M. Salmeron, and M. A. van Hove, Surf. Sci. **418**, 511 (1998).
[52] T. Zambelli, J. Trost, J. Wintterlin, and G. Ertl, Phys. Rev. Lett. **76**, 795 (1996).
[53] J. M. Gallego and R. Miranda. Phys. Rev. B **64**, 085426 (2001).
[54] M. Giesen, F. Schmitz, and H. Ibach, Surf. Sci. **336**, 269 (1995).
[55] A. Brodde and H. Neddermeyer, Surf. Sci. **287/288**, 988 (1993).
[56] S. L. Chang, J. M. Wen, P. A. Thiel, S. Günther, J. A. Meyer, and R. J. Behm, Phys. Rev. B **53**, 13747 (1996).
[57] G. Gilarowski and H. Niehus, Surf. Sci. **436**, 107 (1999).
[58] J. Lindner, P. Poulopoulos, F. Wilhelm, M. Farle, and K. Baberschke, Phys. Rev. B **62**, 10431 (2000).
[59] F. Dulot, B. Kierren, and D. Malterre, Surf. Sci. **494**, 229 (2001).
[60] H. Röder, F. Schuster, H. Brune, and K. Kern, Phys. Rev. Lett. **71**, 2086 (1993).
[61] P. Nouvertné, U. May, M. Bamming, A. Rampe, U. Korte, G. Güntherodt, R. Pentcheva, and M. Scheffler, Phys. Rev. B **60**, 14382 (1999).
[62] J. H. Onuferko, D. P. Woodruff, and B. W. Holland, Surf. Sci. **37**, 357 (1979).
[63] W. Daum, S. Lehwald, and H. Ibach, Surf. Sci. **178**, 528 (1986).
[64] J. Mercer, P. Finetti, F. Leibsle, V. R. Dhanak, R. McGrath, A. Baraldi, K. C. Prince, and R. Rossei, Surf. Sci. **352**, 173 (1996).
[65] H. Onishi, T. Aruga, and Y. Iwasawa, Surf. Sci. **283**, 213 (1993).
[66] J. C. Wood, Jr. and A. J. Nozik, Phys. Rev. B **4**, 2224 (1971).
[67] S. Yu. Grachev, Ph.D. thesis, University of Groningen.
[68] D. Spisak and J. Hafner, Phys. Rev. B **64**, 205422 (2001).
[69] K. E. Johnson, D. D. Chambliss, R. J. Wilson, and S. Chiang, J. Vac. Sci. Technol. A **11**, 1654 (1993).
[70] H. Chatbi, M. Vergnat, Ph. Bauer, and G. Marchal, Appl. Phys. Lett. **67**, 430 (1995).
[71] H. Jiang, Q. L. Wu, K. Tao, and H. D. Li, J. Appl. Phys. **78**, 3299 (1995).
[72] Li Guibin, Li Guoqing, L. Minkai, and L. Bangzhi, Surf. Coat. Technol. **96**, 34 (1997).
[73] E. C. Moreira, L. Amaral, M. Behar, and C. E. Foster, J. Appl. Phys. **80**, 3127 (1996).
[74] H. Chatbi, M. Vergnat, J. F. Bobo, and L. Hennet, Solid State Commun. **102**, 677 (1997).
[75] D. H. Mosca, S. R. Teixeira, P. H. Dionisio, I. J. R. Baumvol, W. H. Schreiner, and W. A. Monteiro, J. Appl. Phys. **69**, 261 (1991).
[76] J. A. Stroscio, D. T. Pierce, and R. A. Dragoset, Phys. Rev. Lett.

70, 3615 (1993).
[77] A. Marciniak, Surf. Eng. **1**, 283 (1985).
[78] H. Du and J. Agren, Z. Metallkd. **86**, 522 (1995).
[79] E. J. Mittemeijer and M. A. J. Somers, Surf. Eng. **13**, 483 (1997).
[80] I. Campos, J. Oseguera, U. Figueroa, and E. Melendez, Surf. Coat. Technol. **102**, 127 (1998).
[81] T. Belmonte, M. Goune, and H. Michel, Mater. Sci. Eng., A **302**, 246 (2001).
[82] J. D. Fast and M. B. Verrijp, J. Iron Steel Inst., London **176**, 24 (1954).
[83] H. Du, L. Sproge, and J. Agren, Modeling of nitrocarburizing, Proceedings of the second ASM Heat treatment and surface engineering, 1993.